# CHAPTER 5: CONTROLLER DESIGN.

## 5.1. INTRODUCTION.

The design and analysis of a linear MPC controller that satisfies the control objectives defined in Chapter 3 will be discussed. The derivation of a linear plant model required for the design of an MPC controller is discussed in detail in Section 5.2. A comparison of the linear and non-linear models is made by means of open loop simulations. The outputs of the linear and non-linear models are thus compared for typical inputs to an EAF under manual control, as described by Bekker [13].

In Section 5.3 an analysis of the open loop system is done to determine the sampling interval to be used for the discrete system. The choices of the MPC tuning parameters and setpoints are discussed in Section 5.4, and a closed loop system analysis is performed in Section 5.5. Some details on the controller implementation are described in Section 5.6, and finally a comparison of the manual and MPC controlled EAFs is done by means of a simulation study.

## 5.2. PLANT LINEARISATION.

### 5.2.1. Model transformation.

The plant model [13] consists of 17 mostly non-linear equations that can be described in the following format:

$$\dot{x}_n(t) = f_n(\mathbf{x}(t), \mathbf{u}(t), \mathbf{d}(t)). \tag{5.1}$$

$f_n$ denotes a non-linear function describing the $n^{th}$ state's change with respect to time, $\mathbf{x}(t)$ is the state vector, $\mathbf{u}(t)$ is a vector of all the manipulated variables (MVs) and $\mathbf{d}(t)$ is a vector of the disturbances. $\dot{x}_n$ is the derivative of the $n^{th}$ state with respect to time.

The linear model required for the controller design needs to be in state space format as described in Equations 5.2 and 5.3.

$$\dot{\mathbf{x}}(t) = \mathbf{A}\mathbf{x}(t) + \mathbf{B}\mathbf{v}(t) \tag{5.2}$$

$$\mathbf{y}(t) = \mathbf{C}\mathbf{x}(t) + \mathbf{D}\mathbf{v}(t) \tag{5.3}$$

The vector, **v**(t), is a combination of the vector of MVs ,**u**(t), and the disturbance vector, **d**(t). For the model considered, the following dimensions apply:

$\mathbf{x}(t) \in \Re^{17x1}$, $\mathbf{y}(t) \in \Re^{7x1}$, $\mathbf{v}(t) \in \Re^{7x1}$.

$\mathbf{A} \in \Re^{17x17}$, $\mathbf{B} \in \Re^{17x7}$, $\mathbf{C} \in \Re^{7x17}$, $\mathbf{D} \in \Re^{7x7}$.

The matrix elements for the linear system can be derived using Equations 5.4 – 5.7, using the principle of a Taylor series expansion [26]:

$$\mathbf{A}(n,m) = \frac{\partial f_n}{\partial x_m}, \tag{5.4}$$

$$\mathbf{B}(n,m) = \frac{\partial f_n}{\partial v_m}, \tag{5.5}$$

$$\mathbf{C}(n,m) = \frac{\partial y_n}{\partial x_m}, \tag{5.6}$$

$$\mathbf{D}(n,m) = \frac{\partial y_n}{\partial v_m}, \tag{5.7}$$

in which $y_n$ is the $n^{th}$ output equation as a function of **x**(t) and **v**(t).

### 5.2.2. Linear model derivation.

A method commonly used in linearising non-linear plants, is to select an equilibrium point, and to linearise the plant at this point using Equations 5.4 – 5.7. This method was used in the first attempt to linearise the plant. Equilibrium or linearisation points were selected by calculating the average values of the states and the inputs (MVs and disturbances) based on plant data of the manually controlled EAF [13]. A simulation was done to compare the linear and non-linear models. A weighed integral square error (ISE) was also calculated for each state and output, by dividing the average error between the linear and non-linear simulations by the range (difference between minimum and maximum values) of the variable in the non-linear simulation. The sum of the weighed ISEs was used as a measure of the accuracy of the linear approximation of the non-linear EAF model.

Although the sum of the weighted ISE is capable of showing the average difference between the linear and non-linear models, it gives no indication of the accuracy of the approximation of each individual variable. An analysis of the individual weighted ISEs and an examination of graphs of the models indicated that some variables, particularly the off-gas temperature and composition, were inaccurately approximated by the linear model. Selecting different linearisation points also failed to solve this problem. Since the off-gas variables are CVs with large cost implications (see Chapter 3), a method was needed to improve the model accuracy. Instead of choosing linearisation points based on expected operating conditions, a gradient algorithm [28] was used to manipulate the matrix elements (of matrices **A**, **B**, **C** and **D**) individually in order to minimise the weighted ISE of the complete model. A block diagram of the gradient algorithm is shown in Figure 5.1.

The weighted ISE of the percentage carbon in the melt didn't show exceptionally large deviations, but the large range of the carbon content increased the complexity of the linearisation. The carbon content is reduced from approximately 3 % at the beginning of the melt to 0.072 % at tapping time [13]. Very small model deviations are thus required close to the tapping time, whilst relatively large variations are initially allowed. This problem was overcome by creating two separate linear models for the carbon content, to be used during different time periods of the simulation.

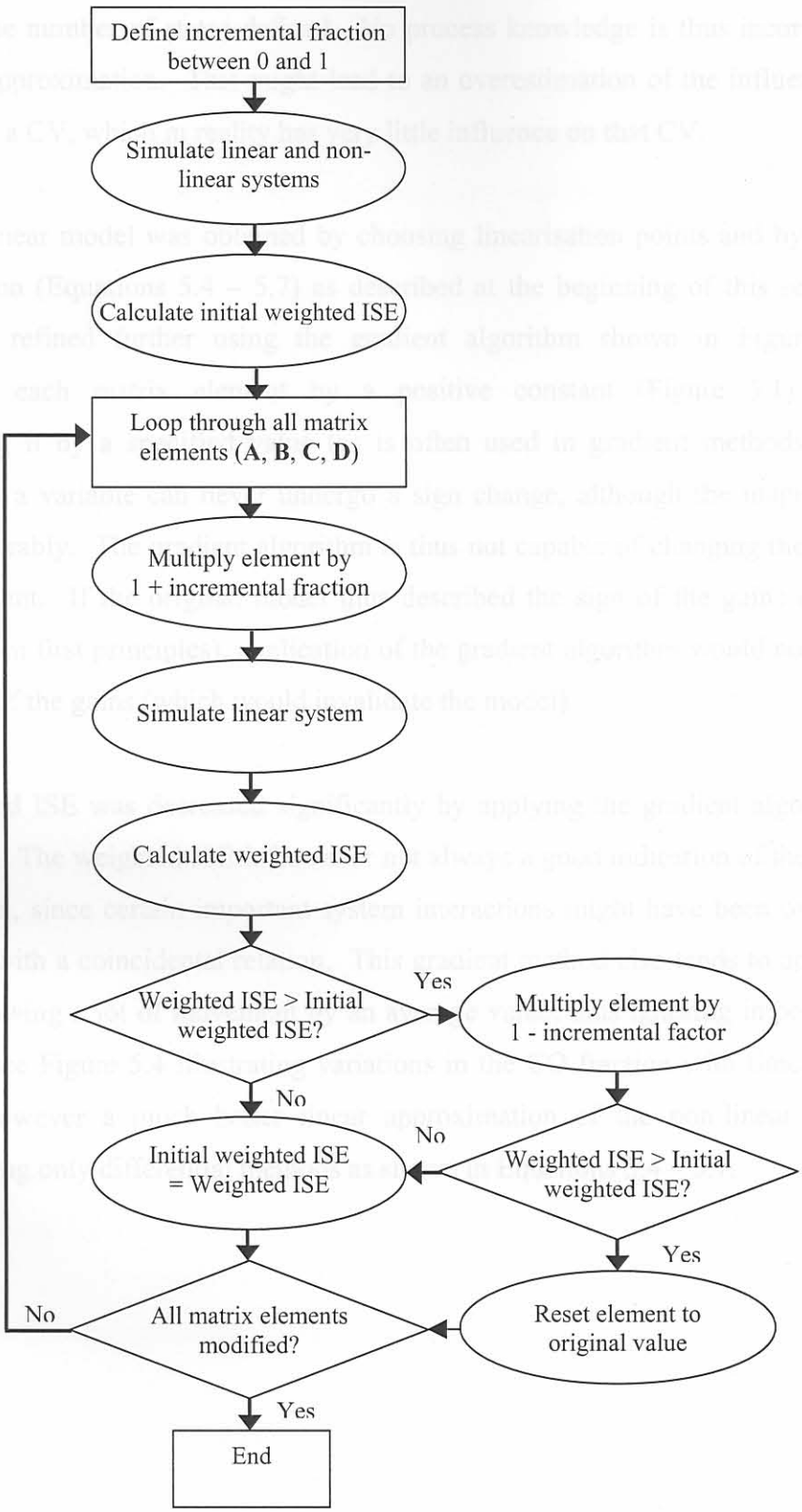


Figure 5.1. Block diagram of the gradient algorithm used to derive a linear model.

This gradient method has the disadvantage that a partial black-box approach is followed, with only the number of states defined. No process knowledge is thus incorporated into the model approximation. This might lead to an overestimation of the influence of some variables on a CV, which in reality has very little influence on that CV.

An initial linear model was obtained by choosing linearisation points and by performing differentiation (Equations 5.4 – 5.7) as described at the beginning of this section. This model was refined further using the gradient algorithm shown in Figure 5.1. By multiplying each matrix element by a positive constant (Figure 5.1) instead of incrementing it by a specified value (as is often used in gradient methods [28]), it is ensured that a variable can never undergo a sign change, although the magnitude might vary considerably. The gradient algorithm is thus not capable of changing the sign of any matrix element. If the original model thus described the sign of the gains correctly (as expected from first principles), application of the gradient algorithm would not change the sign of any of the gains (which would invalidate the model).

The weighted ISE was decreased significantly by applying the gradient algorithm to the two models. The weighted ISE is however not always a good indication of the correctness of the model, since certain important system interactions might have been overlooked or substituted with a coincidental relation. This gradient method also tends to approximate a variable showing a lot of movement by an average value, thus ignoring important system dynamics (see Figure 5.4 illustrating variations in the CO fraction with time). The final model is however a much better linear approximation of the non-linear model than obtained using only differential methods as shown in Equations 5.4 – 5.7.

### 5.2.3. Comparison of linear and non-linear plant models.

Simulations of the linear and non-linear plant models are shown in Figures 5.2 to 5.8 for the 7 CVs, using typical inputs as described by Bekker [13]. The relative furnace pressure, CO fraction and off-gas temperature are measured continuously. Some drift in these variables is therefore not much of a concern since feedback will ensure sufficient corrective action when frequent updates are used. It is however important that these variables should characterise system dynamics accurately, as they will be used for model predictions.

The linear models of relative pressure and off-gas temperature (Figures 5.2 and 5.3) characterise the system dynamics reasonably accurately, although a large drift is observed. Continuous feedback would however easily compensate for this, as is described above. The linear CO-fraction model (Figure 5.4) however contains very little dynamic information, and therefore a large safety margin and a short prediction horizon would be required to account for model inaccuracies. The linear CO-fraction model is in general a bad approximation of the non-linear model, but no linearisation attempt proved effective in improving the accuracy of the linear model. It was therefore decided to use the best obtainable model, but to keep the design specifications conservative to account for model inaccuracies.

The carbon content and liquid metal temperatures are only updated 5 times during the tap. It is thus essential that very little drift is present in these two variables, since the accuracy of any predictions between these updating intervals would depend on the accuracy of these models. Figures 5.5 and 5.6 indicate a good correlation between the linear and non-linear models. Using two models for the carbon content furthermore ensures that a good approximation is obtained for the full duration of the tap.

The steel mass is not measured during the tap, and a good model is thus essential. For the steel mass, linearization using differentiation was preferred over the gradient method, to prevent the possibility of ignoring important system interactions and including coincidental

relations. Figure 5.7 indicates a good correlation between the linear and non-linear models with very little drift.

The linear and non-linear slag foam depth models seem to correlate well, although the influence of the FeO content in the slag is not modelled sufficiently, as can be seen between t = 35 minutes and t = 60 minutes in Figure 5.8. The FeO content in the slag increases from t = 0, reaches a maximum at t = 43 minutes and then decreases until the end of the tap [13]. Depending on the instrumentation, slag foam depth can be measured continuously or at discrete intervals. For these simulations it will be assumed that slag foam depth is updated at the same time intervals as the manual temperature and carbon content measurements, and model inaccuracies might thus necessitate a conservative design strategy.

The combined usage of Taylor approximations for non-linear functions and a gradient algorithm provided a linear model of sufficient accuracy to be used for the design of an MPC controller.

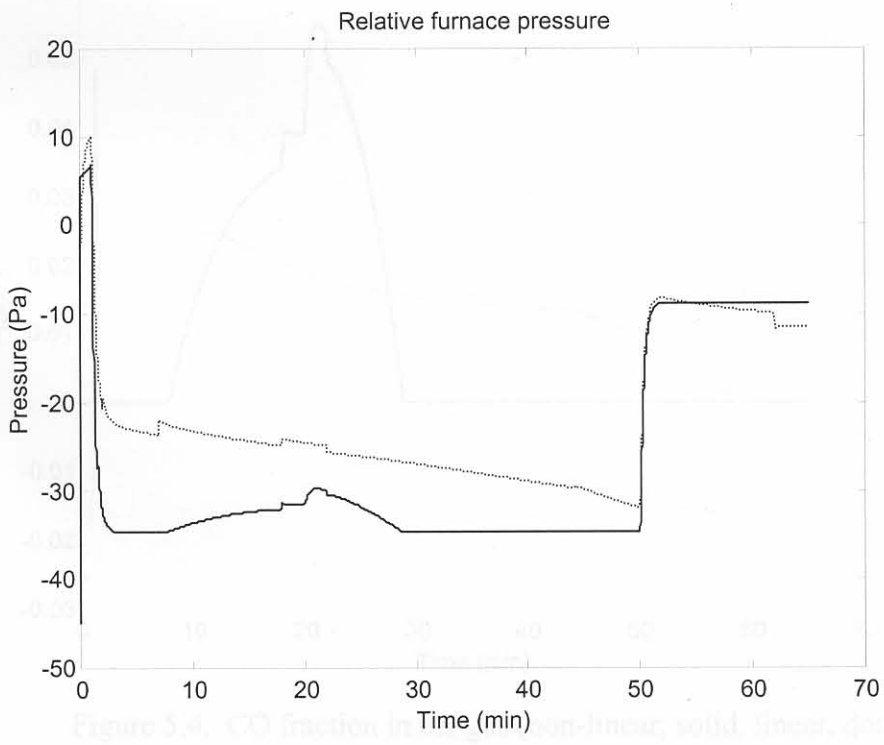


Figure 5.2. Relative pressure (non-linear, solid, linear, dotted).

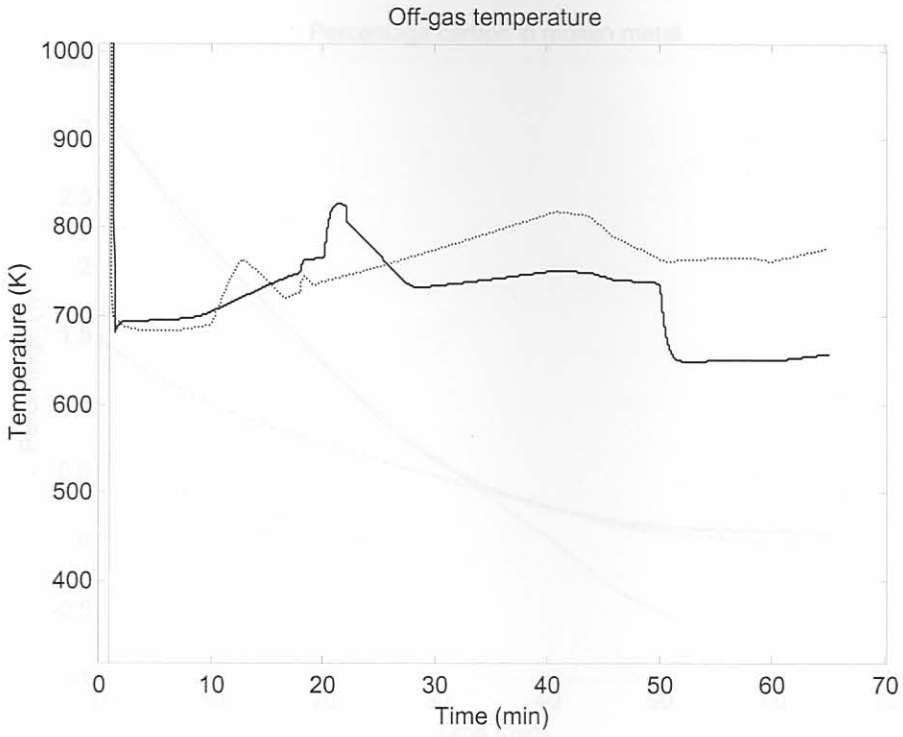


Figure 5.3. Off-gas temperature (non-linear, solid, linear, dotted).

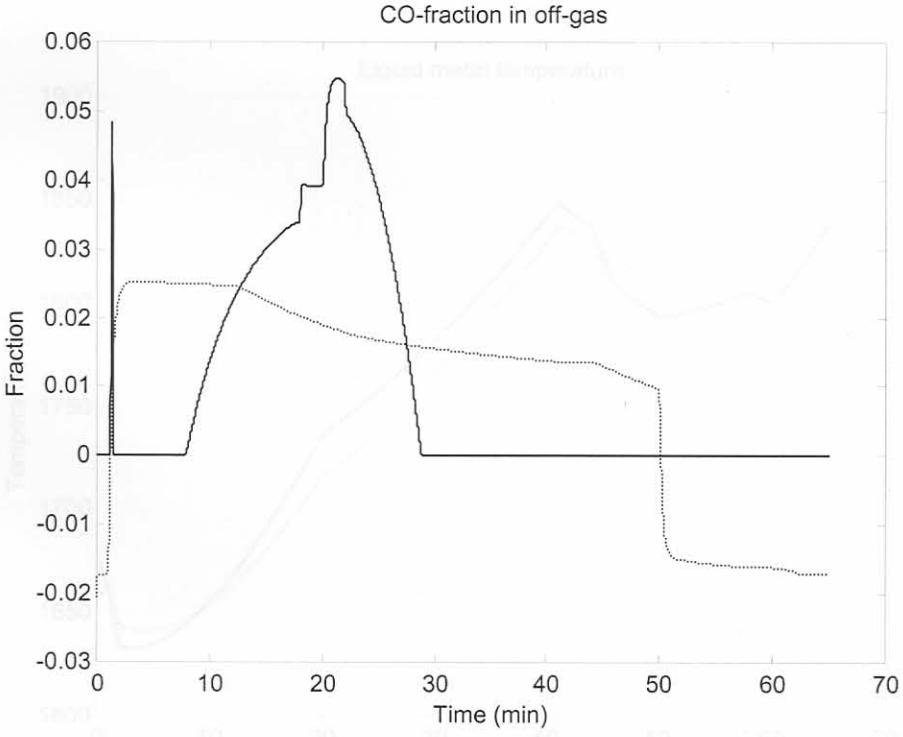


Figure 5.4. CO fraction in off-gas (non-linear, solid, linear, dotted).

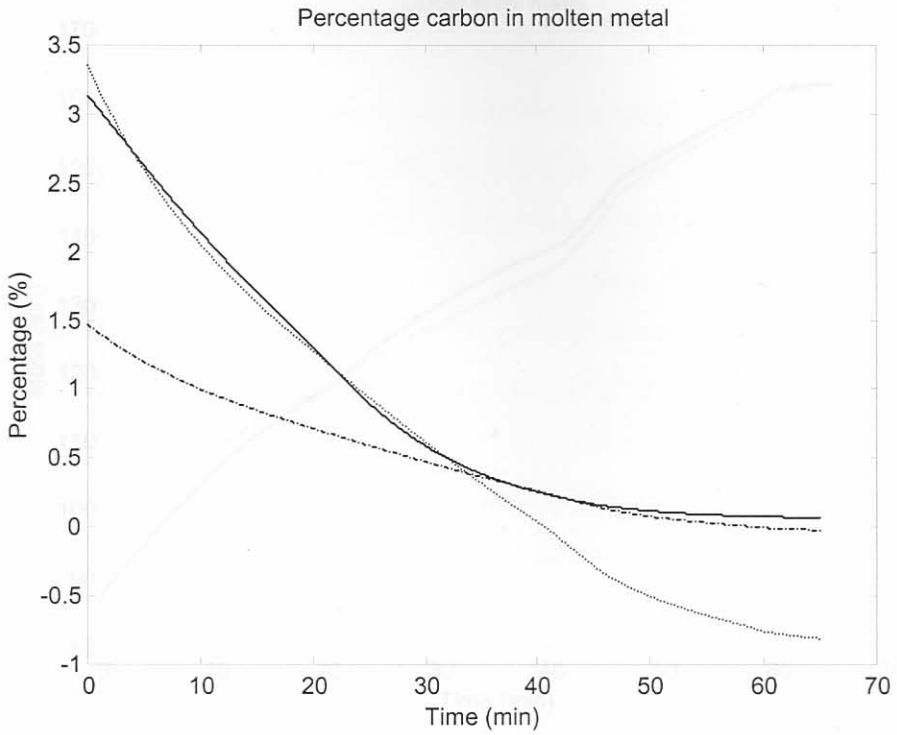


Figure 5.5. Percentage carbon in molten metal (non-linear, solid, linear model for first half, dotted, linear model for second half, dash-dotted).

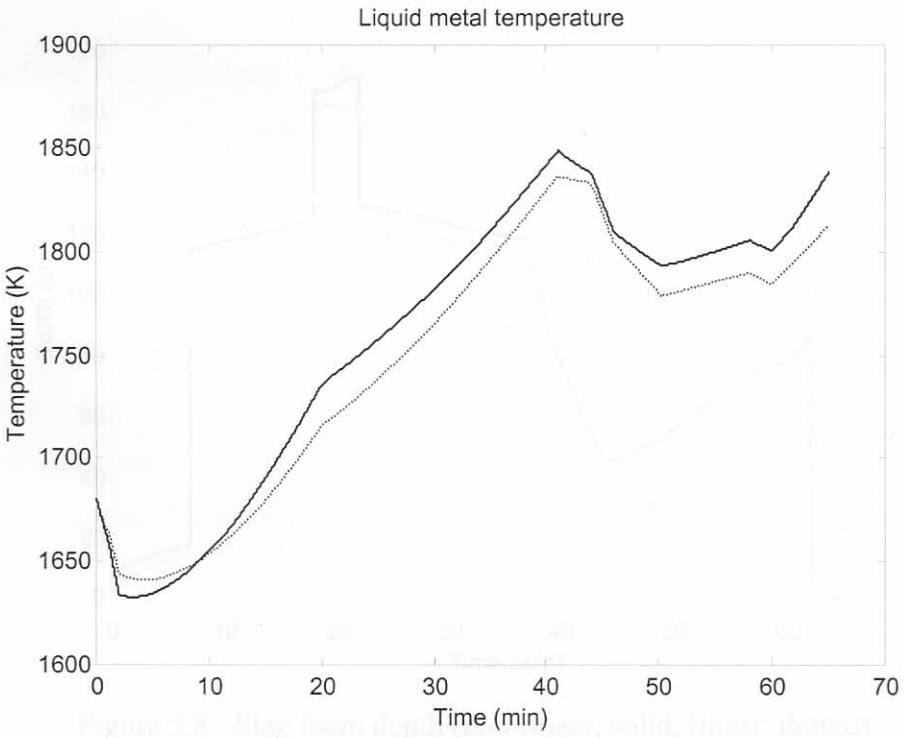


Figure 5.6. Liquid metal temperature (non-linear, solid, linear, dotted).

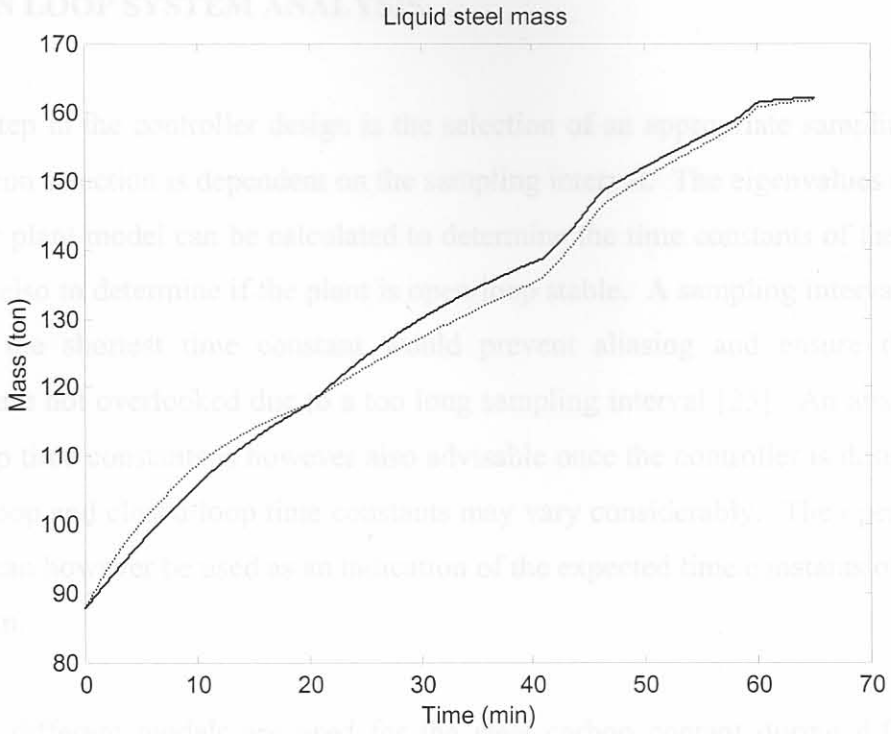


Figure 5.7. Liquid metal mass (non-linear, solid, linear, dotted).

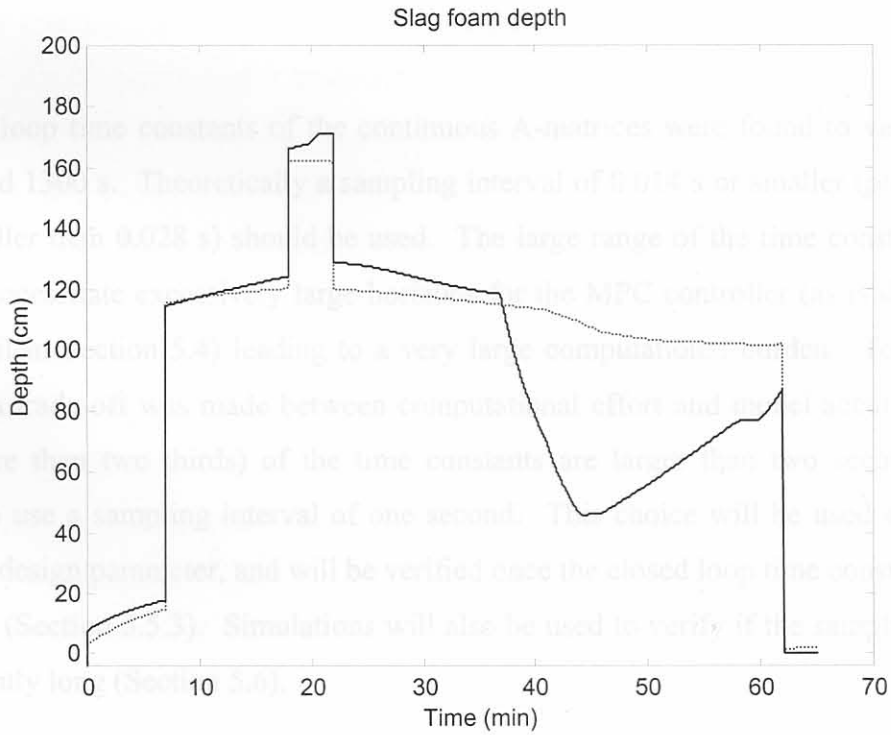


Figure 5.8. Slag foam depth (non-linear, solid, linear, dotted).

## 5.3. OPEN LOOP SYSTEM ANALYSIS.

The first step in the controller design is the selection of an appropriate sampling interval, since horizon selection is dependent on the sampling interval. The eigenvalues of the open loop linear plant model can be calculated to determine the time constants of the open loop plant, and also to determine if the plant is open-loop stable. A sampling interval of shorter than half the shortest time constant would prevent aliasing and ensure that system dynamics are not overlooked due to a too long sampling interval [23]. An analysis of the closed loop time constants is however also advisable once the controller is designed, since the open loop and closed-loop time constants may vary considerably. The open loop time constants can however be used as an indication of the expected time constants of the closed loop system.

Since two different models are used for the steel carbon content during different time frames, the eigenvalues had to be determined for both models. For both models all eigenvalues were found to be smaller than zero, indicating that the system is open loop stable.

The open loop time constants of the continuous A-matrices were found to vary between 0.028 s and 1300 s. Theoretically a sampling interval of 0.014 s or smaller (preferably 10 times smaller than 0.028 s) should be used. The large range of the time constants would however necessitate excessively large horizons for the MPC controller (as is discussed in more detail in Section 5.4) leading to a very large computational burden. To avoid this problem, a trade-off was made between computational effort and model accuracy. Since most (more than two thirds) of the time constants are larger than two seconds, it was decided to use a sampling interval of one second. This choice will be used as an initial controller design parameter, and will be verified once the closed loop time constants can be calculated (Section 5.5.3). Simulations will also be used to verify if the sampling interval is sufficiently long (Section 5.6).

## 5.4. DESIGN PROCEDURE.

The sampling interval chosen in Section 5.3 will be used in the design procedure. The remainder of the design procedure consists of a selection of control (M) and prediction (P) horizons, input- and output weights and also the definition of constraints for the MVs and CVs and the selection of setpoints [21]. These design parameters and final tuning adjustments will be discussed in the following sections.

### 5.4.1. Control and prediction horizons.

Authors seem to differ on initial choices of the prediction horizon, but agree that a large portion of the system response (more than 50 %) should be included in the prediction horizon [23]. The product of the sampling time and the prediction horizon should thus exceed 2.5 times the slowest time constant ($\tau$) (assuming a settling time of $5\tau$). The accuracy of the model used for predictions should however also be considered, since smaller horizons tend to work better with an inaccurate model. Once again the wide range of the time constants and also the accuracy of the model (linear model used to control a non-linear plant) require that a trade-off be made. It was found that most of the time constants are below 20 seconds, suggesting a prediction horizon of 50. Some trial and error tuning showed that a prediction horizon of 25 provided adequate control. A shorter prediction horizon led to sustained oscillation due to a limited prediction interval in the presence of model uncertainty. Higher values of the prediction horizon frequently lead to an infeasible quadratic problem, since model inaccuracies drove the non-linear EAF model into an infeasible region (exceeding the maximum off-gas temperature), whilst the linear EAF model predicted that the EAF would remain inside the feasible region. This was mainly due to modelling inaccuracies in the off-gas temperature and the fact that a hard constraint was specified to prevent the off-gas temperature from exceeding the maximum specified temperature.

For inaccurate models a small control horizon is usually suggested [23]. Simulation studies indicated that M = 5 is a good choice, but M = 3 resulted in a controller much more robust to unmeasured disturbances. It was decided in favour of the more robust controller (M = 3), although control tended to become much more sluggish.

### 5.4.2. Constraints on manipulated variables.

Constraints were specified on the MVs to ensure that they are only manipulated within their typical operational ranges. These operational ranges were determined by examining plant data [13] and also through private communication [18]. The minimum and maximum ranges of the MVs are shown in Table 5.1. The minimum limit on the off-gas fan was specified to prevent model inaccuracies when the off-gas flow-rate approaches zero. From a process perspective, the specification of a lower safety limit on the off-gas fan is also feasible, as this would prevent the build-up of gasses inside the EAF due to insufficient off-gas flow-rates. No limit was placed on the rate of change of the MVs, but the selection of weights in Section 5.4.4 serves the purpose of suppressing excessive movement in the control actions.

Table 5.1. Constraints on MVs.

| MV | Minimum | Maximum |
|---|---|---|
| Off-gas fan power. | 0.1 MW | 2 MW |
| Slip-gap width. | 0 m | 0.6 m |
| Oxygen injection rate. | 0 kg/s | 5 kg/s |
| DRI addition rate. | 0 kg/s | 35 kg/s |
| Graphite addition rate. | 0 kg/s | 1 kg/s |

### 5.4.3. Constraints on controlled variables.

Constraints were placed on the CVs to prevent the model from exceeding physical limitations (e.g. a mass becoming negative). The maximum constraints were in general specified much larger than the maximum values obtainable by the CVs, and can thus be

approximated as infinity (∞). These maximum constraints (approximated as ∞) are of little significance for the controller since they are never reached.

Two exceptions to the constraints mentioned above are the constraints placed on the off-gas temperature and slag foaming depth. The minimum limit of the off-gas temperature was set to 300 K due to physical temperature constraints. A maximum constraint of 760 K was specified to ensure that the off-gas would never exceed the maximum specification of 773 K (500°C), thereby including a small safety factor of 13 K. This upper limit was thus not based on physical constraints, but was chosen to satisfy the control objective on the off-gas temperature. This furthermore made the specification of an off-gas temperature setpoint and weight unnecessary, since no cost implication is associated with any off-gas temperature between 300K and 773 K.

Similar to the specification on the maximum off-gas temperature, a minimum limit was specified for the slag foaming depth. No benefit or disadvantage is associated with a slag foaming depth higher than 30 cm. Energy transfer to the melt only decreases if the slag foam depth is lower than 30 cm. Due to modelling inaccuracies, the slag foam depth of the non-linear model decreased below 30 cm although the linear model showed a sufficient depth. To prevent this from occurring in the absence of feedback, the minimum constraint on the slag foaming depth was increased to 50 cm, which yielded satisfactory results. No maximum constraint was specified for the slag foaming depth (∞), but the increasing cost of the feed materials prevents the slag foam depth from becoming excessive. In reality the height of the furnace or another opening in the furnace (e.g. slag door) would limit the maximum height of the slag layer.

For a system with more CVs than MVs, better control often results from specifying fixed setpoints only for variables where good regulation is required, whilst allowing other variables to float between certain limits. For the EAF under consideration much improved control was obtained, especially on the other off-gas variables, by relaxing the weights on the off-gas temperature and slag foaming depth, and specifying limits. A summary of the constraints on the CVs used in the controller is given in Table 5.2.

Table 5.2. Constraints on CVs.

| CV | Minimum | Maximum |
|---|---|---|
| Relative furnace pressure. | - ∞ | 0 Pa |
| Off-gas temperature. | 300 K | 760 K |
| CO-fraction in off-gas. | 0 | 1 |
| % Carbon in steel. | 0 % | 100 % |
| Steel temperature. | 300 K | ∞ |
| Steel mass. | 0 kg | ∞ |
| Slag foam depth. | 50 cm | ∞ |

### 5.4.4. Weights.

The selection of proper weights is crucial for this controller since the economic impact of each CV is reflected by its weight. An inaccurate choice of weights will cause the objective function to differ from the real costs experienced on the plant, and would prevent the real cost of EAF operation from being minimised. The objective function as shown in Chapter 4 is in the form of Equation 5.8 [20], with weights on the CVs indicated by $\mu_j$ and weights on variations in the MVs indicated by $\lambda_j$. The weights on the MVs serve the purpose of suppressing oscillation and excessive movement of the MVs. These weights should be chosen as small as possible to minimise their contribution to the objective function [23], and are typically found by trial and error.

$$J = \sum_{j=N1}^{P} \mu_j (r(t+j) - \hat{y}(t+j \mid t))^2 + \sum_{j=1}^{C} \lambda_j \Delta u(t+j-1)^2 \qquad (5.8)$$

Additional to the CVs defined previously, 5 other CVs were defined to represent the MVs. This was necessary since the objective function does not consider absolute values of the MVs (only variations), although the absolute values of the MVs determine their cost contribution to the tap. Only $\mu_j$ is thus used to specify the economic objectives whilst $\lambda_j$ is used to increase stability.

In Chapter 3, the control objectives defined in Chapter 2 were translated into percentages of operating cost, as a function of deviation of the CVs from their setpoints. The relative cost contribution of the MVs were also tabulated in Chapter 3. To minimise the cost of the MVs, the setpoints for all the MVs were chosen equal to zero. Table 5.3 gives the per unit percentages for the MVs in the unit that feed rate is typically specified. These values, divided by the ranges of the MVs as specified in Table 5.1, were used as the $\mu_j$ values for the CVs corresponding to the MVs.

Table 5.3. The cost contribution of feed materials under typical operating conditions.

| MV | Cost contribution | Per unit cost | Unit |
|---|---|---|---|
| Off-gas fan power. | 0.58 % | 0.725 % | /MW |
| Slip-gap width. | 0 % | 0 % | /m |
| Oxygen feed rate. | 0.7 % | 0.54 % | /kgs$^{-1}$ |
| DRI feed rate. | 9.18 % | 1.1 % | /kgs$^{-1}$ |
| Graphite feed rate. | 0.1 % | 2.895 % | /kgs$^{-1}$ |

The next step is to translate the economic implication of not reaching the setpoints on the CVs into similar per unit percentages. The costs defined in Chapter 3 need to be transformed into a form similar to the objective function given by Equation 5.8. This was done by linearising the economic implication over the ranges the CVs are expected to vary. A straight line was thus fitted between the minimum and maximum cost contributions of each CV for the expected range of each CV, and the gradient of the line calculated to represent the per-unit cost. An example follows:

Equation 5.9, which describes the percentage increase in the cost of a tap as a function of deviation from the tapping temperature setpoint (see Chapter 3), is an example of a non-linear cost function that needs to be linearised.

$$\begin{aligned} \Delta\%\text{Cost} &= 8\,\% + 0.063\,\% \cdot (\text{abs}(\Delta T) - 10) \ldots \text{for abs}(\Delta T) > 10 \\ \Delta\%\text{Cost} &= 0 \qquad\qquad\qquad\qquad \ldots \text{for abs}(\Delta T) < 10 \end{aligned} \tag{5.9}$$

$\Delta$%Cost describes the percentage increase in operating cost if the tapping temperature differs more than 10 K from the setpoint. If the tapping temperature is within 10 K of the setpoint, no corrective action is required and $\Delta\%\text{Cost}_{min}$ = 0 %. If it is assumed that the maximum tapping temperature deviation from the setpoint would be approximately 50 K, $\Delta\%\text{Cost}_{max}$ = 10.52 %. The gradient of the increase in cost due to deviation from the tapping temperature setpoint is thus 10.52 % / 50 K = 0.2104 %/K, as shown in Table 5.4. A steel temperature 50 K below the setpoint at tapping would thus increase the cost of the tap by 10.52 %.

The expected maximum ranges of the CVs, the economic implication at the maximum deviation (calculated using the assumptions in Chapter 3) and the per-unit costs are shown in Table 5.4. The per-unit costs shown in Table 5.4, divided by their maximum ranges, were used for the $\mu_j$ values corresponding to the CVs.

Table 5.4. The economic implication of not reaching control objectives.

| CV | Maximum range | Cost at max. | Per unit cost | Unit |
|---|---|---|---|---|
| Relative pressure. | 5 Pa | 0.628 % | 0.1256 % | /Pa |
| Off-gas temperature. | 100 K | 3 % | 0.03 % | /K |
| CO emission. | 0.1 % | 1000 % | 10 000 % | /CO fraction |
| Carbon content. | 0.001 % | 10 % | 10 000 % | /%C |
| Steel temperature. | 50 K | 10.52 % | 0.2104 % | /K |
| Steel mass. | 18 t | 10 % | $5.55\text{x}10^{-4}$ % | /kg |
| Foamy slag depth. | 30 cm | 0.9 % | 0.03 % | /cm |

Although the objective function as given by Equation 5.8 is quadratic, most costs described in Chapter 3 are linear functions, whilst the non-linear costs are linearised as described above. The fact that a quadratic objective function, as given in Equation 5.8, is used to represent a linear cost function is no reason for concern as a transformation can easily be made. The ISE between a linear function of the format $y_1 = k_1x$ and a quadratic function of the format $y_2 = k_2x^2$ ($k_2 = \mu_j$, $x^2 = (r-y)^2$) over a defined range, $x_{max}$, is minimised by choosing $k_2 = 5/(4k_1x_{max})$. The derivation of this relation follows.

Assume that a linear function, $y_1$, is represented by Equation 5.10, and a quadratic function, $y_2$, is represented by Equation 5.11.

$$y_1 = k_1 x \tag{5.10}$$

$$y_2 = k_2 x^2 \tag{5.11}$$

The objective is to minimise $(y_1 - y_2)^2$ over the range $x_{min}$ to $x_{max}$, by calculating an appropriate relation between $k_1$ and $k_2$. The ISE is given by Equation 5.12. As $y_1$ and $y_2$ are symmetrical, the calculation can be simplified by choosing $x_{min} = 0$, which yields Equation 5.13.

$$ISE = \int_{x_{min}}^{x_{max}} (y_1(x) - y_2(x))^2 \, dx \tag{5.12}$$

$$ISE = \frac{1}{3}k_1^{\,2}x_{max}^{\,3} - \frac{1}{2}k_1k_2x_{max}^{\,4} + \frac{1}{5}k_2^{\,2}x_{max}^{\,5} \tag{5.13}$$

By differentiating the ISE with respect to $k_2$ and setting the derivative equal to zero, the values of $k_1$ and $k_2$ that would minimise the ISE can be calculated, as shown in Equation 5.14.

$$\frac{dISE}{dk_2} = -\frac{1}{2}k_1x_{max}^{\,4} + \frac{2}{5}k_2x_{max}^{\,5} = 0 \tag{5.14}$$

The ratio between $k_1$ and $k_2$ that would minimise the ISE can now be calculated, as shown in Equation 5.15.

$$k_2 = \frac{5}{4} k_1 / x_{max} \tag{5.15}$$

In many cases the quadratic representation (Equation 5.11) is a more accurate representation of the real cost implication than the linear approximation (Equation 5.10), since a small deviation in general has a very small cost implication whilst a large deviation in general has a much larger implication.

### 5.4.5. Setpoints.

Setpoints were chosen to correspond with values obtained from the manually controlled EAF. For the relative pressure, a setpoint of 0 Pa was specified, since this would minimise energy losses in the off-gas stream, without compromising the safety of workers. The relative pressure never approached the critical level of 0 Pa in the simulation study (Figure 5.12). The setpoints for the CO-fraction in the off-gas necessitated a much lower relative pressure to avoid the build-up of CO inside the EAF. Depending on the specific operating conditions on a plant, a lower relative pressure setpoint may be specified if it is found that the relative pressure frequently tends to become positive. The weight, $\mu_j$, may also be modified to account for the cost implication of positive relative pressure, rather than for the cost of excessive energy wastage, as used in this simulation study.

The setpoint for the CO-fraction was set equal to zero, since this would minimise the possibility of legislative action due to excessive CO emission.

The carbon setpoint was specified as an exponential function starting at 3.14 % and ending at 0.072 %. The setpoint has a time constant of 975 seconds, implying that 4 time constants elapse during a tap. A comparison of the setpoints, the manually controlled variables and the MPC controlled variables are shown in Section 5.6.

The setpoint for the liquid metal temperature is based on the temperature profile of the manually controlled EAF. The setpoint is 1680 K during the first 10 minutes of the simulation. Between t = 10 minutes and t = 40 minutes, the temperature setpoint increases linearly to 1850 K. For the remainder of the simulation the setpoint remains at 1850 K, which is also the tapping temperature (see Figure 5.16).

The setpoint for the liquid steel mass is a linear function increasing from 87925 kg to 162110 kg. The initial steel mass is based on the liquid metal present inside the EAF when the automatic control can commence (after scrap has been melted partially and hot metal added [13]). The setpoint for the final steel mass at tapping time is identical to the final steel mass obtained under manual control.

The setpoints for the off-gas temperature and slag foam depth are not of much importance as the constraints specified on these two variables make setpoint following unnecessary. The weights, $\mu_j$, on these two variables were also reduced by a factor of 1000 to prevent these variables from contributing significantly to the objective function (other than when reaching constraints). The weights were not reduced to zero since this tends to cause numerical instability in the minimisation function. Setpoints were therefore specified as 500 K and 50 cm respectively, although their influence on the objective function is negligible.

For the MVs modelled as CVs, setpoints were specified equal to zero. This was done to ensure that as little as possible of the feed materials or energy inputs are used during the steelmaking process, subject to other cost implications and constraints. The only exception is the slip-gap width, as a larger slip-gap opening has no direct cost implication, but indirectly influences the off-gas fan power required to maintain a certain relative pressure. A small weight, $\mu_j$, however takes care of this and the setpoint was kept at zero.

### 5.4.6. Additional tuning.

Modification of the weights described in Section 5.4.4 should be avoided, as this would reduce the accuracy of the EAF cost model. The accuracy of the cost model described by the objective function in Equation 5.8, can however in some cases be increased. This is possible if the assumptions implicit to the derivation of the weights are invalidated in a certain operating region, or if limitations of the objective function reduces model accuracy.

One such case was already discussed in Section 5.4.3, where the weights of the slag foam depth and off-gas temperature were reduced by a factor of 1000, and limits specified within which these two variables are allowed to vary. The accuracy of the cost model was increased considerably by this step, as the quadratic objective function (Equation 5.8) is symmetrical, whilst the off-gas temperature only contributes to the cost if it exceeds a maximum value, and the slag foam depth only if it is lower than a minimum value.

Another modification to the weights suggested in Section 5.4.4 was made to the weights on the steel temperature and carbon content. The weights for these two CVs were calculated assuming typical specifications at tapping. At any other stage during the tap, the steel temperature and carbon content is however of little importance. Due to the large range of the carbon content, the weight should ideally vary inversely proportional to the carbon content, as was simulated by Viljoen [10]. A simpler approach was followed by specifying two different weights for the two different controllers used during the two time frames for which the different carbon models were defined in Section 5.2.3. The weight of the carbon content was thus reduced by a factor of 10 during the first half of the simulation, whilst the steel temperature weight was increased by a factor of 10. During the second half of the simulation, the original weights were used, as the assumptions used in deriving these weights are more accurately approximated closer to tapping time.

To avoid invalidating the cost model, further tuning was limited to choosing appropriate weights on variations in the MVs ($\lambda_j$) to ensure stability. Minor adjustments were made to the tapping temperature weight to improve setpoint following, but the objective function of final controller remains an accurate mapping of the cost model described in Chapter 3.

## 5.5. CLOSED LOOP SYSTEM ANALYSIS.

Analysis methods for non-linear systems are restricted to systems satisfying specific conditions, and very often simulations are the only method of analysing complex non-linear systems. The simulations shown in Section 5.6 indicate that the system is stable and that control objectives are met. A single simulation is however not sufficient in proving stability or good setpoint following, and a more rigorous analysis method is required.

For a linear system without constraints, numerous tools exist to characterise the system properties [23,27,29]. An approximation of the properties of a non-linear system, based on a linear approximation, is however only valid in the region where the two models are accurately matched. A comparison of the open-loop linear and non-linear models (Section 5.2.3) indicates that a good linear approximation of a non-linear system can be obtained. With the exception of the off-gas temperature and slag foaming depth, constraints on the CVs are either irrelevant or not reached under typical operational conditions (see Section 5.6) and the MVs also seldom reach their constraints. Instead of drawing conclusions on a single simulation study, it was decided to analyse the properties of the closed loop system more thoroughly by using the linear model without constraints.

A constant MPC gain matrix can be calculated for a linear unconstrained system, using the methods and functions described in [21]. Since two different linear models were used, two different MPC gain matrices would result, and the analysis would be based on both these models. The closed loop transfer function of the MPC controlled EAF can be determined from the MPC gain matrix and the linear system [21], which can be used for further analysis. The limitations of the approximation however need to be taken into account and will be discussed where applicable.

### 5.5.1. Stability.

The stability of the closed loop system can be analysed by calculating the eigenvalues of the closed loop **A**-matrix. Since a discrete implementation of the controller is used, the system would be stable if all the eigenvalues are within the unit circle [27]. For both models the absolute value of the maximum eigenvalue was smaller than 1, which implies that the system is stable. This conclusion may be invalidated if some non-linearity forces the system into an unstable region, but since the linear and non-linear models seem to correlate well, this is unlikely.

### 5.5.2. Frequency domain analysis.

The frequency domain analysis of the system was performed using singular value decomposition (SVD) [29]. Similar to Bode plots used for single-input single-output (SISO) systems, singular values give an indication of the system gain at specific frequencies for multiple-input multiple-output (MIMO) systems. For MIMO systems the gain would however not only depend on the frequency, but also on the direction of the input-vector. The SVD plot would thus consist of two lines indicating the minimum and maximum system gain at a specific frequency, for different input vector directions.

For the closed loop system, the inputs would correspond to the setpoints and the outputs to the system outputs. The direction of the setpoint-vector would thus vary as different setpoint combinations are specified. For good setpoint following, the SVD plot must have two properties: Firstly, the gain must be close to unity (or 0 dB) for the frequency band in which good setpoint-following is required. This would ensure an exact mapping from the setpoints to the outputs. The second requirement is that the minimum and maximum singular values must not differ significantly within this frequency band. Large variations between the minimum and maximum singular values would imply that the gain (and thus the mapping from the setpoints to the outputs) varies significantly as the direction of the setpoint vector changes, which is clearly undesirable.

The Matlab functions: mod2frsp.m and svdfrsp.m was used to generate the SVD plots. These two functions also allow specification of the inputs and outputs to be included in the analysis. Various combinations of CVs can thus be analysed to determine which combinations would yield good setpoint following and which not.

Figure 5.9 shows an SVD plot of all 7 CVs: Relative furnace pressure, CO fraction in off-gas, off-gas temperature, percentage carbon in steel melt, liquid metal temperature, liquid metal mass and slag foam depth. It can be seen that significant differences exist between the minimum and maximum singular values. Simulation studies confirmed that poor setpoint following is obtained when attempting to control all 7 CVs. This can be explained by noting that the EAF has 7 CVs and only 5 MVs. The controller thus attempts to satisfy all 7 control objectives by manipulating only 5 MVs. The deviations of the CVs from their setpoints are based on the relative weights in order to minimise the objective function. Good regulation is not achieved on any of the CVs, and control is in general very ineffective.

This problem was partly overcome by relaxing the weights on the off-gas temperature and slag foaming depth, as discussed in Section 5.4.6. This implies that 5 MVs can now be used to control 5 CVs, unless the off-gas temperature or slag foam depth are close to their constraints. A linear analysis excluding slag foam depth and off-gas temperature would also give a more accurate representation of the non-linear system, since the variables that reach their constraints would be omitted from the analysis. An SVD plot is shown in Figure 5.10, illustrating the frequency domain analysis of 5 of the CVs, excluding the off-gas temperature and slag foam depth. It can be seen that the difference between the minimum and maximum singular values decreased considerably, but the difference is still unacceptably large and the gain at low frequencies is far from 0 dB.

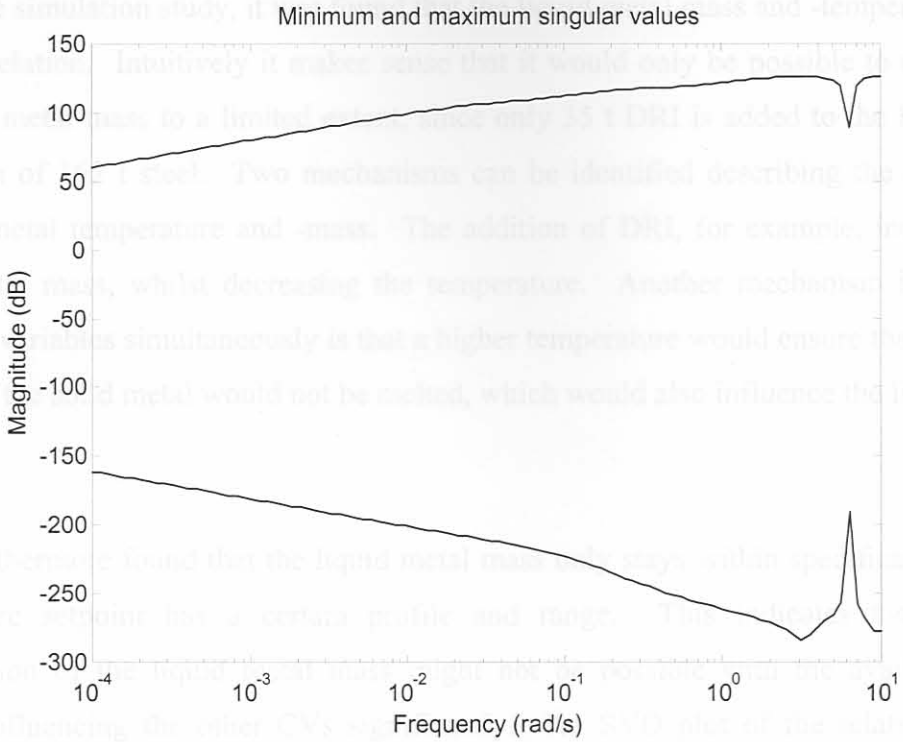


Figure 5.9. SVD plot for all seven CVs.

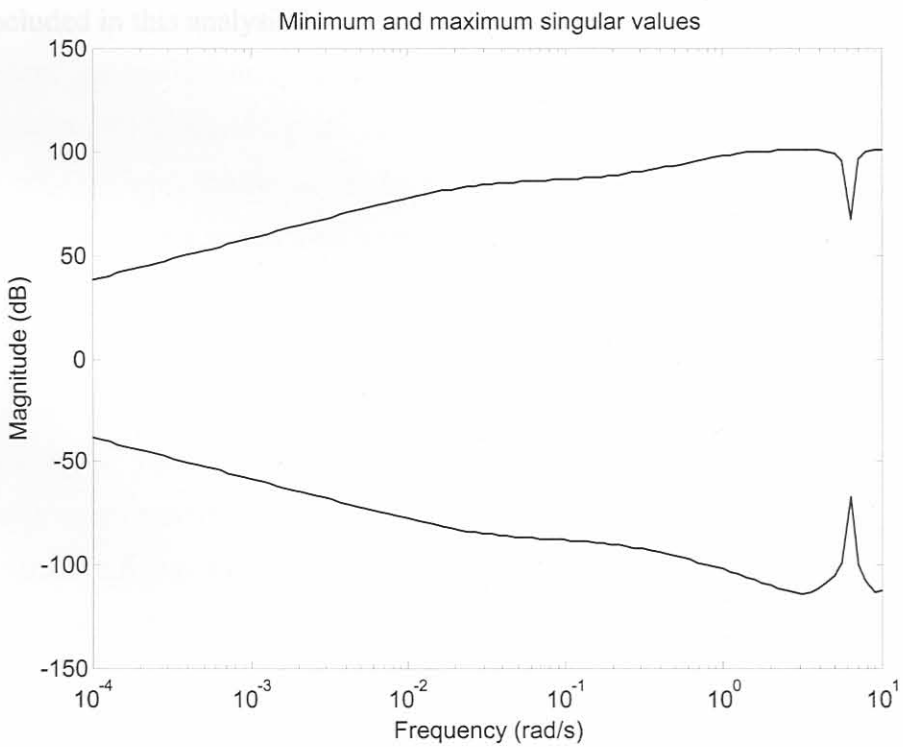


Figure 5.10. SVD plot for 5 CVs (excludes off-gas temperature and slag foam depth).

During the simulation study, it was found that the liquid metal mass and -temperature have some correlation. Intuitively it makes sense that it would only be possible to manipulate the liquid metal mass to a limited extent, since only 35 t DRI is added to the EAF in the production of 162 t steel. Two mechanisms can be identified describing the correlation between metal temperature and -mass. The addition of DRI, for example, increases the liquid metal mass, whilst decreasing the temperature. Another mechanism influencing these two variables simultaneously is that a higher temperature would ensure that a smaller portion of the solid metal would not be melted, which would also influence the liquid metal mass.

It was furthermore found that the liquid metal mass only stays within specifications if the temperature setpoint has a certain profile and range. This indicates that efficient manipulation of the liquid metal mass might not be possible with the available MVs without influencing the other CVs significantly. An SVD plot of the relative furnace pressure, CO fraction in off-gas, percentage carbon in steel and liquid metal temperature is shown in Figure 5.11. The slag foam depth, off-gas temperature and liquid metal mass are thus not included in this analysis.

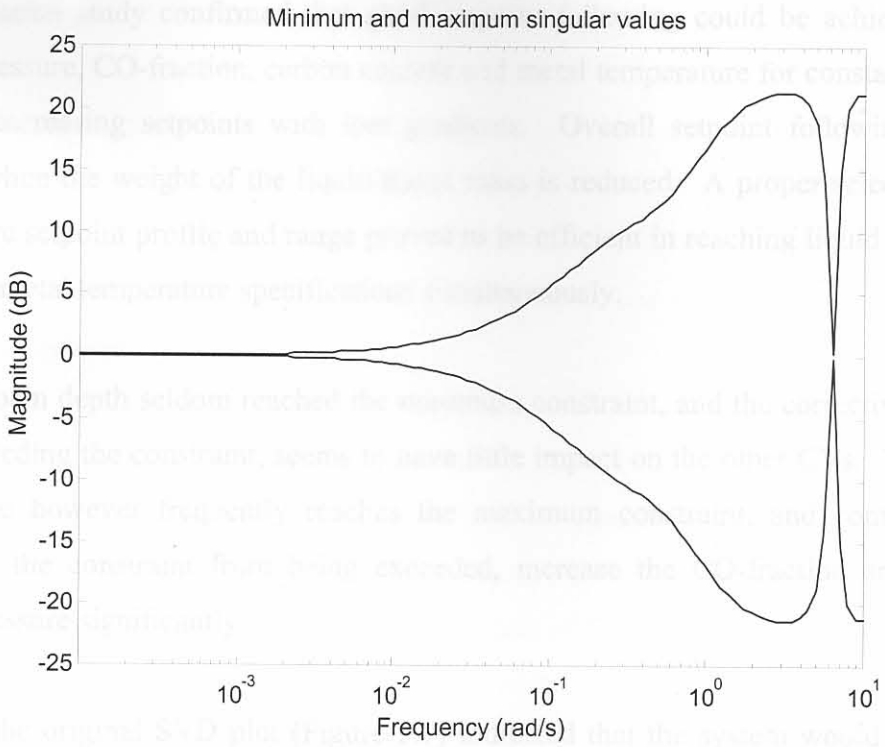


Figure 5.11. SVD plot for relative pressure, CO-fraction, percentage carbon in steel and steel temperature.

The minimum and maximum singular values are very close together for all frequencies below 0.1 rad/s. At higher frequencies the singular values vary considerably (more than 6 dB) and poor setpoint following can be expected. The EAF is a slow varying process and most of the setpoints can be kept constant for the duration of the tap. Setpoint changes slower than 0.1 rad/s would be tracked efficiently by the four CVs analysed, and good setpoint following can be expected in this frequency range.

The large singular values at high frequencies however also imply that high frequency measurement noise would be amplified, potentially degrading system performance. The adaptive nature of the MPC controller should however be sufficiently effective to compensate for the non-ideal system characteristics.

The simulation study confirmed that good setpoint following could be achieved on the relative pressure, CO-fraction, carbon content and metal temperature for constant setpoints or linear increasing setpoints with low gradients. Overall setpoint following seem to improve when the weight of the liquid metal mass is reduced. A proper selection of the temperature setpoint profile and range proved to be efficient in reaching liquid metal mass and liquid metal temperature specifications simultaneously.

The slag foam depth seldom reached the minimum constraint, and the corrective action to avoid exceeding the constraint, seems to have little impact on the other CVs. The off-gas temperature however frequently reaches the maximum constraint, and control actions preventing the constraint from being exceeded, increase the CO-fraction and also the relative pressure significantly.

Although the original SVD plot (Figure 5.9) indicated that the system would show poor setpoint following, some adjustments to the system configuration (adding constraints, relaxing weights and specifying suitable setpoints) proved to be efficient in designing a system capable of reaching control objectives, as is suggested by Figure 5.11.

### 5.5.3. Sampling interval verification.

A sampling interval was chosen in Section 5.3 based on the time constants of the open loop system. As the time constants can vary considerably between open- and closed loop systems, a verification of the sampling interval is recommended to ensure that the controller is capable of capturing system dynamics. The discrete closed loop system was transformed into a continuous system, and the eigenvalues of the continuous closed loop **A**-matrix was used to determine the time constants. Similar to the open loop time constants, the closed loop time constants vary over a wide range, from 0.04 s to times exceeding the tapping time. More than half the time constants are however longer than 2 seconds, and using the same reasoning as given in Section 5.3, a sampling interval of 1 second is still considered a good trade-off between computational effort and accuracy of the discrete model, although not an ideal choice.

## 5.6. CONTROLLER IMPLEMENTATION.

The performance of the MPC controlled EAF was compared to that of the manually controlled EAF under typical operating conditions as described by Bekker [13]. The simulation was done in Microsoft Visual C++. This simulation study serves the purpose of showing that the controller is functionally effective, whilst a more thorough economic evaluation is presented in Chapter 7.

A linear MPC controller was implemented to control the non-linear plant described by Bekker [13]. This was done to represent a typical situation existing in industry where significant differences might exist between the plant and the model used by the controller. The non-linear model is also a better representation of the real EAF and results based on the non-linear plant model would thus be more accurate than results based on the linear model. The linearised model as described in Section 5.2 was therefore implemented as an internal model for the controller, whilst the complete non-linear model was used to simulate plant behaviour and to provide feedback to the controller where applicable. The constraints defined in Section 5.4 were used in both the linear and non-linear models, and the rest of the controller tuning was implemented as described in Section 5.4.

To ensure that the simulation is a realistic representation of reality, only continuous measurements (relative furnace pressure, off-gas temperature and CO-fraction in off-gas) are fed back to the controller continuously. Measurements of the carbon content and temperature of the liquid metal are only taken approximately 5 times during a tap [18]. For the simulation study these values are used as feedback to the controller only at the following discrete time intervals: t = 30, 45, 53, 59 and 64 minutes, based on plant data [13]. Slag foam depth is also updated at these 5 discrete intervals, although some plants have continuous measurements available. The liquid metal mass is not measured during the tap and no feedback is thus provided.

A comparison of the CVs under MPC and manual control is shown in Figures 5.12 – 5.18. Some prominent effects due to actions taken under manual control is highlighted and a complete discussion of the data used for manual control can be found in Bekker [6].

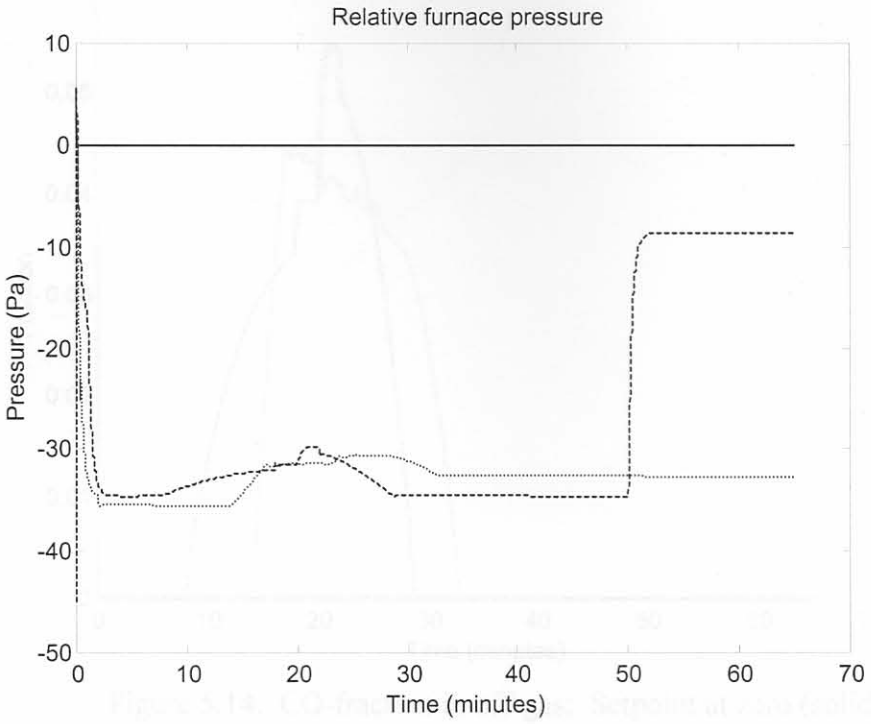


Figure 5.12. Relative furnace pressure: Setpoint (solid), Manual control (dashed) and MPC (dotted).

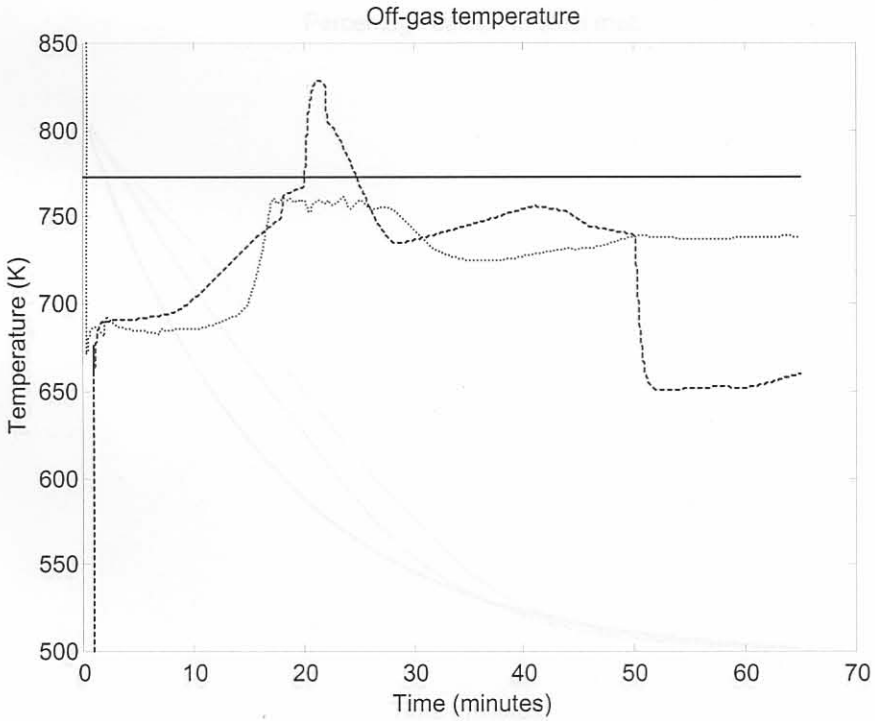


Figure 5.13. Off-gas temperature: Maximum limit (solid), Manual control (dashed) and MPC (dotted).

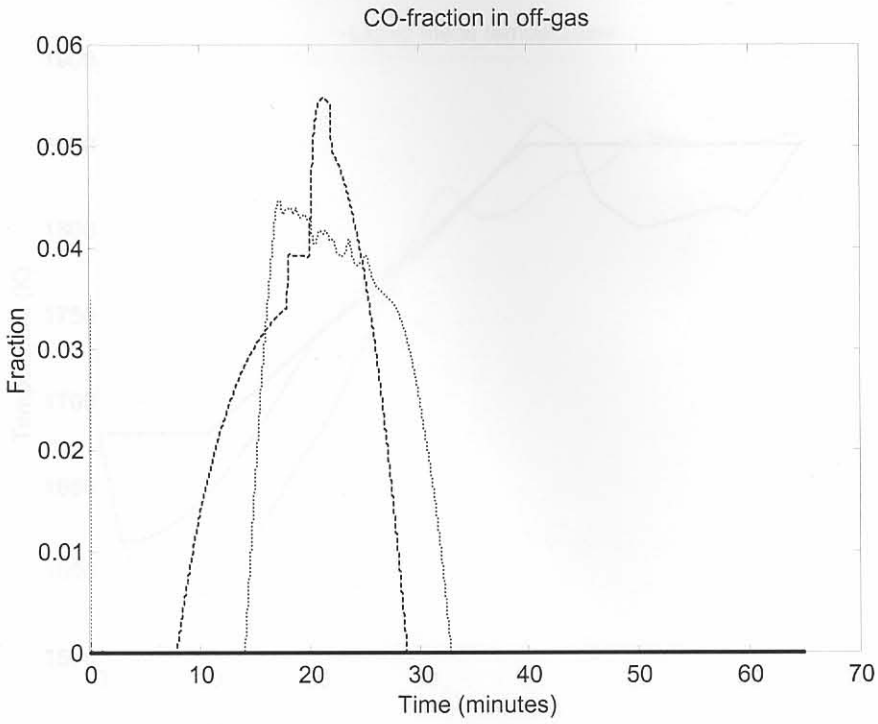


Figure 5.14. CO-fraction in off-gas: Setpoint at zero (solid), Manual control (dashed) and MPC (dotted).

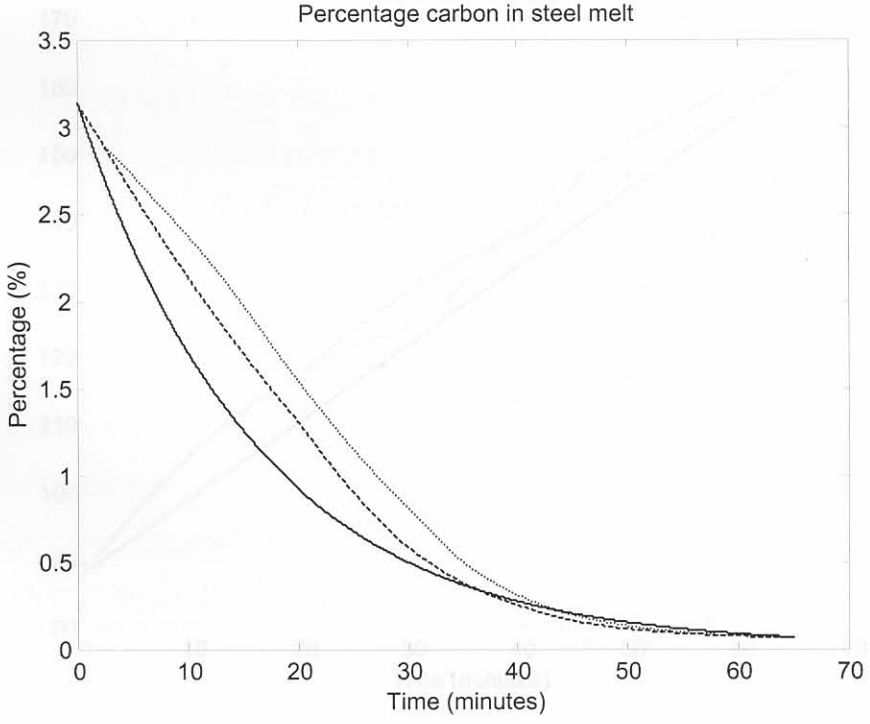


Figure 5.15. Percentage carbon in steel melt: Setpoint (solid), Manual control (dashed) and MPC (dotted).

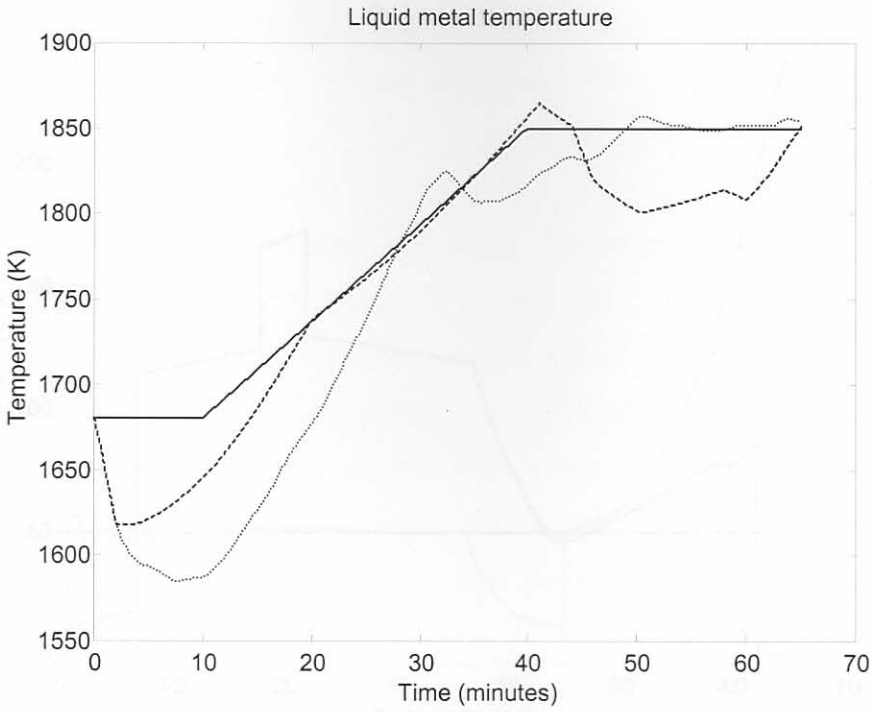


Figure 5.16. Liquid metal temperature: Setpoint (solid), Manual control (dashed) and MPC (dotted).

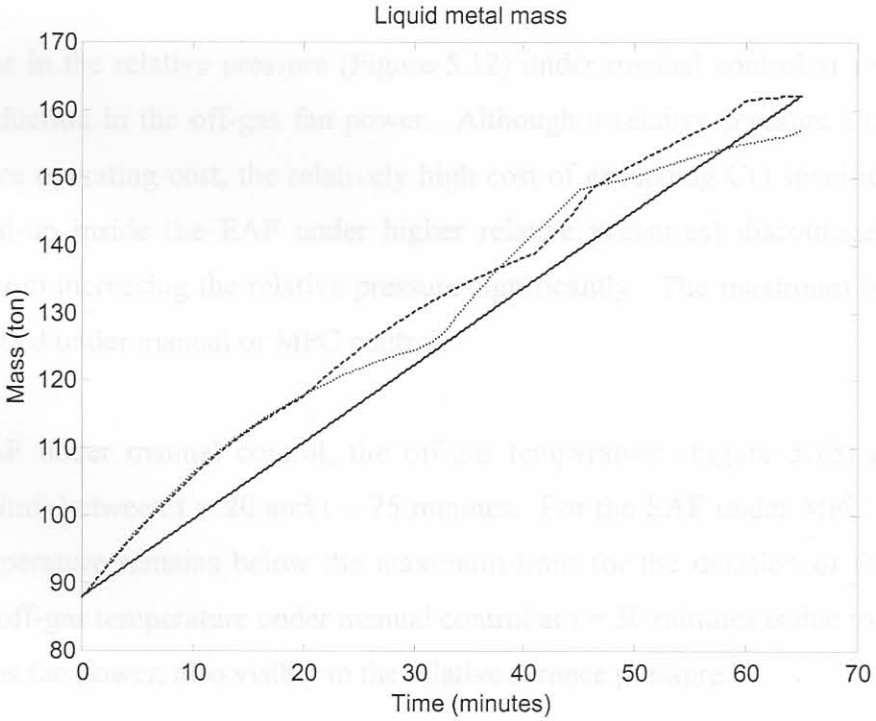


Figure 5.17. Liquid metal mass: Setpoint (solid), Manual control (dashed) and MPC (dotted).

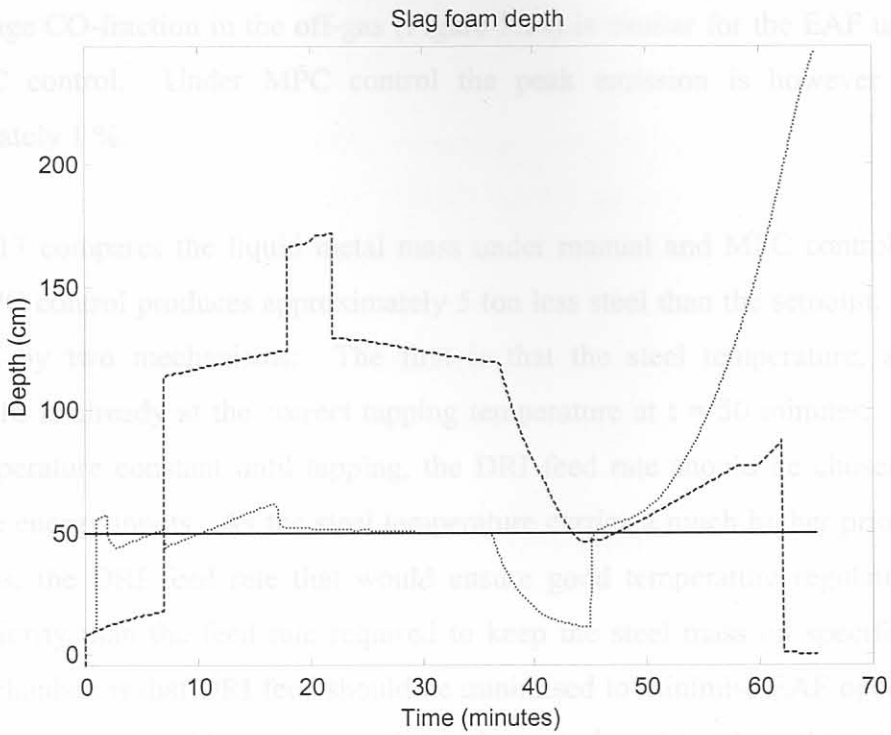


Figure 5.18. Slag foam depth: Setpoint (solid), Manual control (dashed) and MPC (dotted).

The increase in the relative pressure (Figure 5.12) under manual control at t = 50 min is due to a reduction in the off-gas fan power. Although a relative pressure closer to 0 Pa would reduce operating cost, the relatively high cost of exceeding CO specifications (due to CO build-up inside the EAF under higher relative pressures) discourages the MPC controller from increasing the relative pressure significantly. The maximum limit of 0 Pa is not exceeded under manual or MPC control.

For the EAF under manual control, the off-gas temperature (Figure 5.13) exceeds the maximum limit between t = 20 and t = 25 minutes. For the EAF under MPC control, the off-gas temperature remains below the maximum limit for the duration of the tap. The drop in the off-gas temperature under manual control at t = 50 minutes is due to a reduction in the off-gas fan power, also visible in the relative furnace pressure.

The average CO-fraction in the off-gas (Figure 5.14) is similar for the EAF under manual and MPC control. Under MPC control the peak emission is however reduced by approximately 1 %.

Figure 5.17 compares the liquid metal mass under manual and MPC control. The EAF under MPC control produces approximately 5 ton less steel than the setpoint. This can be explained by two mechanisms: The first is that the steel temperature, as shown in Figure 5.16 is already at the correct tapping temperature at t = 50 minutes. To keep the steel temperature constant until tapping, the DRI feed rate should be chosen such as to match the energy inputs. As the steel temperature carries a much higher priority than the steel mass, the DRI feed rate that would ensure good temperature regulation carries a higher priority than the feed rate required to keep the steel mass on specification. The other mechanism is that DRI feed should be minimised to minimise EAF operational cost. The cost associated with producing 5 ton less steel is less than the additional cost associated with charging an additional 5 tons of DRI, thus explaining the reduced DRI consumption and accompanying reduction in steel mass.

At t = 44 minutes, the percentage carbon in the steel melt dropped below the setpoint (Figure 5.15). The controller attempts to correct this error by injecting more graphite into the slag, thereby indirectly increasing the steel carbon content. The increased graphite injection however causes the slag foam depth to increase out of bounds from t = 44 minutes (Figure 5.18), as only a lower limit was specified for the slag foam depth (no penalization for higher foam depths). The slag foam depth would in reality only increase up to a level where overflowing would occur, but specification of an upper limit for the graphite injection rate should be capable of preventing this from occurring. The steps visible in the slag foam depth under manual control (between t = 0 and t = 30 minutes) are due to step changes in the graphite injection rate. The reduction in the slag foam depth from t = 36 minutes and the subsequent increase from t = 43 minutes, can mainly be attributed to the FeO content of the slag. The slag FeO content reaches a maximum at t = 43 minutes and then decreases until tapping. The inverse relation between the slag foam depth and the slag FeO content is clearly visible under manual control, but worsen the slag foam depth runaway under MPC control further.

## 5.7. CONCLUSION.

The design and analysis of an MPC controller was discussed and a simulation study presented comparing an EAF under manual control to one under MPC control. The controller reaches all control objectives whilst reducing the peak CO emission and maximum off-gas temperature compared to manual control. A much more thorough analysis of the economic feasibility of the MPC controller will be undertaken in Chapter 7, but functionally MPC proves being effective in controlling the EAF.